DOI: 10.1002/ ((please add manuscript number))
Article type: Full Paper

High-Fluorinated Electrolytes for Li-S Batteries

*Jing Zheng, Guangbin Ji, Xiulin Fan, Ji Chen, Qin Li, Haiyang Wang, Yong Yang, Kerry C. DeMella, Srinivasa R. Raghavan, Chunsheng Wang**

J. Zheng, Dr. X. Fan, Dr. J. Chen, Q Li, Dr. H. Wang, Y. Yang, Dr. S. R. Raghavan, Prof. C. Wang
Department of Chemical and Biomolecular Engineering
University of Maryland, College Park, MD 20742, USA
E-mail: cswang@umd.edu
J. Zheng, Dr. G. Ji
College of Materials Science and Technology, Nanjing University of Aeronautics and Astronautics, Nanjing 210016, P. R. China
K. C. DeMella
Department of Chemistry and Biochemistry
University of Maryland, College Park, MD 20742, USA

Keywords: inert fluorinated diluents, localized high-concentration electrolyte, polysulfide shuttle, lithium dendrite, Li-S batteries

Abstract:

Rechargeable Li-S batteries have been regarded as one of the most promising next-generation energy-storage systems. However, the inevitable formation of Li dendrite and the shuttle effect of lithium polysulfides significantly weakens the electrochemical performance, preventing its practical applications. Herein, we report a new class of localized high-concentration electrolyte (LHCE) enabled by adding inert fluoroalkyl ether of 1H,1H,5H-octafluoropentyl-1,1,2,2-tetrafluoroethyl ether (OFE) into high-concentrated electrolytes (HCE) LiFSI/DME system to suppress Li dendrite and minimize the solubility of the high-order polysulfides in electrolytes, thus reducing the amount of electrolyte in cells. Such a unique LHCE can achieve a high coulombic efficiency of Li plating/stripping up to 99.3% and completely suppression of shuttling effect, thus maintain S cathode capacity of 775 mAh/g for 150 cycles with a lean electrolyte of 4.56 g/Ah. The LHCE reduces the solubility

of lithium polysulfides, allowing Li/S cell to achieve super performance in a lean electrolyte. This conception of using inert diluents in highly concentrated electrolyte can accelerate commercialization of Li-S battery technology.

1. Introduction

Owing to the high natural abundance of elemental sulfur, high theoretical cell capacity of 1667 mAh/g, and theoretical cell energy density of 2510 Wh/kg, rechargeable Lithium-sulfur (Li-S) batteries have been regarded as a promising alternative to state-of-the-art lithium-ion batteries (LIBs) for energy storage applications.[1] However, current Li-S batteries still face several serious challenges, including "shuttle" reaction due to the dissolution of polysufides (Li_2S_n, n>4) in electrolytes and dendritic Li growth on Li anode, which significantly lower the cell coulombic efficiency (CE) and cycling performance.[2] In addition, the lithium polysulfides dissolution and Li dendrite growth also require a large amount excess electrolyte to achieve high performance, thus reducing the energy density. Extensive efforts have been devoted to suppress "shuttle" of lithium polysulfide. Among them, encapsulating sulfur cathode into porous host materials including porous carbon[3], metal oxide/chalcogenide[4], and conductive polymers[5] are the most effective method for suppressing "shuttle" effect. On the Li anode side, nanostructure design [6] or surface modification[7] have been also developed to suppress the dendritic Li growth.

Different from separately nanostructured design of the electrodes, rational design and optimization of electrolytes are more effective,[8] which simultaneously suppress both lithium polysulfide shuttle and Li dendrite.[9] Recently, highly concentrated electrolyte (HCE) systems with unique solvation structure and functionality have been successfully developed for high performance Li-S batteries. For example, Suo et al. showed a new class of ultrahigh salt concentration electrolyte, which can effectively suppress the lithium dendrite growth and

inhibit the polysulfide shuttle phenomenon in Li-S batteries.[2c] Qian et al. reported that the high-concentration electrolytes enabled the high-rate cycling of lithium metal with a high CE up to 99.1% without dendrite growth [2a]. These significant performance improvements were contributed to the strong restraining property for the solvents from the high-concentrated salts in electrolyte that efficiently control the reaction dynamics and Li_2S_n solubility synchronously. These exciting breakthroughs demonstrated that such unique HCE systems can offer new possibilities to address the shuttle effect and dendritic Li growth efficiently and simultaneously.

Nevertheless, the usage of a large amount of expensive lithium salt in the HCE systems also lead to several disadvantages, including high cost, poor wettability, high viscosity and low ionic conductivity.[10] To address these issues without scarifying the unique characteristics of HCE, a new kind of localized high-concentration electrolyte (LHCE) was proposed by using a rational cosolvent dilution in HCE system. The choice of the cosolvent in LHCE is critical for the performance of Li-S batteries. In Li-S battery electrolytes, ether-based solvents with high donor number were usually employed, which can effectively dissociate the Li^+ from anion and dissolve Li salts. However, the strong donating ability of such solvents can also facilitate the dissolution of long-chain polysulfide and amplify the negative influence from the “shuttle effect”. Therefore, a “inert” cosolvent with low donor ability, permittivity, electrolyte viscosity but high wettability is required for the LHCE, which can maintain the Li^+ solvation structure complexes in HCE and suppress the polysulfide solubility but with significantly reduced salt usage. For example, 1,1,2,2-tetrafluoroethyl-2,2,3,3-tetrafluoropropyl ether (HFE) was employed as the diluent solvent in HCE for Li-based batteries which not only maintain the original Li^+-solvent complex but also lower the electrolyte concentration higher wettability and lower viscosity[11] allowing to use less

electrolyte. Furthermore, the choice of the "inert" cosolvent must consider the formation of SEI layer which can significantly affect the cycling performance and lifetime of the battery. As the analogous to HFE, the solvent of 1H,1H,5H-octafluoropentyl-1,1,2,2-tetrafluoroethyl ether (OFE) with lower flammability but higher fluorination degree are identified to better suit for the "inert" solvent requirements, which can be used to dilute the ether-based HCE to obtain the LHCE system for Li-S battery.

In this work, a new "inert" cosolvent, the inert cosolvent of OFE was employed to develop a novel ether-based electrolyte system (LiFSI/OFE+DME) for Li-S batteries. By adjusting the volume percentage of OFE in these OFE-based electrolytes, the polysulfide shuttle of Li-S cells can be effectively suppressed. The Li-S cells in a lean 1M LiFSI/OFE+DME5 electrolyte (4.56 g/Ah) shows a stable cycle performance with the capacity retention of 775 mAh/g at 100 mA/g after 150 cycles. The high average CE of 99.2% for S cathodes, and a high stripping/plating CE of 99.3% for Li anodes demonstrate lithium polysulfide dissolution and dendritic Li growth have been effectively suppressed. In addition, 1M LiFSI/OFE+DME5 electrolyte is nonflammable, which is promising for next generation safe and high-performance Li-S batteries.

2. Results and Discussion

2.1. Physicochemical Properties of Electrolytes

Lithium bis (trifluoromethane sulfonyl) imide (LiTFSI) is the most commonly used metal salt for Li-storage batteries. As the analogous to LiTFSI, lithium bis (fluorosulfonyl) imide (LiFSI) possesses the similar structures with LiTFSI but better ion mobility/conductivity property and higher labile fluorine, leading to the more formation of F-rich anion-originated interphase. In this work, three OFE-based electrolytes with the LiFSI salt was designed, 1M LiFSI/OFE+DME with an OFE/DME volume ratio of 50/50, 85/15,

and 95/5 were prepared, denoted as DME50, DME15, and DME5, respectively. Traditional 1M LiTFSI/DOL+DME (denoted as DOL+DME) was also employed as the reference electrolyte. The physicochemical properties of ionic conductivity, Li^+ transference number and viscosity for these electrolytes were first investigated, as shown in **Figure 1a-b**. The ionic conductivity of traditional DOL+DME electrolyte is about 9.40 mS/cm, which is in good agreement with the previous reports, [2c, 12] For the OFE-based electrolytes, the ionic conductivity reduced gradually with the increasing volume ratio of OFE, maintaining a value of 5.23 mS/cm for DME50 electrolyte, 1.94 mS/cm for DME15 electrolyte, and 1.24 mS/cm for DME5 electrolyte (**Figure 1a**). In the mixed solvent of DME and OFE, the Li^+ is preferentially solvated with DME molecules, and the inert OFE solvent is scarcely involved in the solvation with Li^+. Therefore, the dissociation of Li salt and the number of charge carriers in these OFE-based electrolytes increased along with the increased volume ratio of DME from DME5, DME15 to DME50 electrolyte, which is consistent with the previously reported results. [13] Different from ionic conductivity, the Li^+ transference number increases with the decreasing volume ratio of DME in electrolytes from 0.17 for DME50, 0.22 for DME15 to 0.28 for DME5. This tendency was determined by the existential forms of Li^+ in these electrolytes. In the electrolyte with enough DME, the excess DME molecules can replace the bound of FSI^- to form solvent-separated ion pairs (SSIPs), leading to a large existence of free FSI^- anion which effectively suppress the Li^+ transference speed. As the decreasing volume ratio of DME, it exists with different forms of solvate complexes from contact ion pairs (CIPs, an FSI^- coordinating with one Li^+) to the aggregates (AGGs, an FSI^- coordinating with two or more Li^+, no free FSI^-), leading to less resistance of Li^+ migration from the FSI^-. [14] As a result, the increasing Li^+ transference number as the decreasing of DME volume ratio can partially compensate the loss of ion conductivity in the OFE-based electrolytes.

As another important parameter for electrolytes, their viscosities were measured as a function of shear-rate, as shown in **Figure 1b**. The data demonstrate that the viscosities are almost independent of shear-rate (top in **Figure 1b**), indicating that the fluids are Newtonian in their rheological behavior (much like water). Therefore, each electrolyte can be characterized by a single viscosity value, as shown by the bar graph in the bottom of **Figure 1b**. DOL+DME exhibits the highest viscosity of 3.7 mPa.s among all the electrolytes studied; in comparison, the OFE-based electrolytes have lower viscosities and the viscosity of DME5 is the lowest of the lot (2.4 mPa.s). The viscosities of DME15 (2.6 mPa.s) and DME50 (3.3 mPa.s) are also lower than that of DOL+DME. The low viscosity of OFE-based electrolytes ensures high power density and high utilization of active materials in Li-S cells.

Digital photos for the solubility of Li_2S_8 in various solvents and electrolytes are shown in **Figure 1c**. In line with previous reports, [15] the solubility of Li_2S_8 in the solvent of DME is high, appearing with dark red color; but in OFE, no obvious color can be observed with tiny solubility. Owing to the high solubility of Li_2S_8 in DOL and DME solvents, the color of 1M LiTFSI/DOL+DME electrolyte mixed with Li_2S_8 also displays the dark red color. Obviously; in the three OFE-based electrolytes, the color gets lighter from dark brown, light yellow, to colorless along with the decreasing ratio of DME, indicating a significant reduce of polysulfide solubility from the DME50, DME15 to DME5 electrolyte. The corresponding UV-Vis spectra for these electrolytes with saturated Li_2S_8 are demonstred in **Figure 1d**. The characteristic absorption peaks located at about 220 nm and 270 nm can be attributed to the signal of DME solvent and presence of S_8, respectively; the signals for both DME and S_8 can be observed in all the solvents and electrolytes, which is due to existence of the electrolyte solvent (DME) and raw material (the mixing of Li_2S and S_8) for the preparation of Li_2S_8 polysulfide solution. However, it can be clearly seen that the profile of Li_2S_8 signal at around

424 nm gets smaller and smaller with the decreasing of DME ratio from DME50 to DME15 and totally disappears in DME5 electrolyte. Similarly, Li_2S_8 signal at around 424 nm is also not obseerved in the inert OFE solvent (**Figure S1**). Therefore, this positive results suggest that the dissolution of lithium polysulfide is stepwise controlled by the introduction of inert OFE cosolvent into the LiFSI/DME electrolytes.

2.2. Flammability of OFE-based Electrolytes

The safety issue such as flammability of the organic ether-based electrolytes in Li-S batteries is also a critical obstacle for the wide application of Li-S batteries. Herein the ignition and combustion behaviors of different solvents and elelctrolytes are also evaluated, as displayed in **Figure 2** and **Video S1-2**. As displayed in **Video S1**, the inert fluorinated OFE solvent cannot be ignited, while DME can burn very rapidly once ignited, which can be attributed to the lower vapor pressure (7.42 mmHg) but higher boiling point (~133 ^{o}C) and flash point (45.037 ^{o}C) of OFE than that of DME (**Table S1**). When removing the heat-source from the objectives, there is no observable flame for OFE (**Figure 2a**) but still exuberant flame for DME (**Figure 2b**). **Figure 2c** shows the maximum flame size for each electrolyte, along with its correponding images of glass-fiber after combustion. It can be observed that the flame of OFE-based electrolyte is getting smaller as the increase of OFE content from DME50, DME15 to DME5, indicating that the OFE in these electrolytes improves the nonflammability of the electrolytes. It is so difficult to ignite the electrolyte of DME5, even with multiple tries of ignition; while for the electrolytes of DOL+DME, DME50, and DME15, they can burn very rapidly with much brighter flame (**Video S2**). Furthermore, the color of glass-fiber after combustion (inset in **Figure 2c**) is white for the 1M LiTFSI/DOL+DME reference electrolyte, but it is black for all OFE-based electrolytes. The white color of glass-fiber with 1M LiTFSI/DOL+DME reference electrolyte indicates a complete combustion

event of electrolyte occurs with sufficient flammable DME solvent, on the contrast, the black glass-fiber is attributed to the incomplete combustion of the OFE-based electrolytes. It seems that the glass-fiber color in DME50 is slightly more black than that in DME5, which may be owing to the inefficient burning for higher volume ratio DME in DME50 under the same air contact. These results manifest that the introduction of nonfalmmablity OFE can reduce the flembility of the electrolytes for safe Li-S battery applications.

2.3. Li Metal Plating/Stripping Cycling CE and Stability

Li|Cu cells were then employed to investigate the Li stripping/deposition stability in these electrolytes (**Figure 3**). As demonstrated in **Figure S2**, the Li|Cu cells in the LHCE of DME5 show very high CE of 99.3% for 250 cycles at a current of 1 mA cm^{-2} with the deposition capacity of 1.0 mAh cm^{-2}. The voltage profile of Li metal plating/stripping in DME5 at different cycles (**Figure 3a**) and different current densities (**Figure 3b)** shows that the Li plating/stripping in DME5 electrolyte is highly stable, and voltage hysteresis just slightly increase with the increasing of current densities. Even at a high current rate of 8 mA cm^{-2}, a stable process for Li stripping/planting also can be received with a high CE of 94.7%. However, under the same current of 1 mA cm^{-2} and the same deposition capacity of 1.0 mAh cm^{-2}, the CE of the dilute DME50 electrolyte is only 83% with rapid fade after 250 cycles (**Figure 3c-d**). This can be ascribed to the solid electrolyte interphase (SEI) formed from reduction of DME-OFE solvent in DME50 is not robust enough to suppress the Li dendrite growth.

The deposition morphology of Li metal surface after 100 deposition/stripping cycles in Li|Cu cells in the OFE-based electrolytes was examined by SEM without exposing to air, as demonstrated in **Figure 3e**. Obviously, a nodule-like Li deposition surface without any dendrite growth is obtained in the DME5 elecrolyte, but some tiny and spiculate Li dendritic

growths can be obviously observed on the surface of Li metal in the DME15 elecrolyte, and much worse in DME50 elecrolyte. Moreover, the size of Li nodule in DME5 is larger than the size of Li dendrite in the elecrolyte of DME15 and DME50, demonstrting that the SEI formed in DME5 electrolyte sucesfully supressed the Li dendrite formation during Li stripping/plating.[10a]. The larger particle size with Li smooth nodule in DME5 can effectively reduce contact area with the electrolyte, minimizing the parasitic reactions and prolonging the cycle stability.

Moreover, the polarization test of Li|Li symmetric cells in the OFE-based electrolytes was further performed to investigate the long term compatibility and cycling stability, as indicated in **Figure S3**. The cycling performance of Li|Li cells in DME5 electrolyte at a current density of 1 mA cm^{-2} and a deposition capacity of 1.0 mAh cm^{-2} shows a very stable cycling profile without any voltage polarization increment even after 600h cycling (**Figure S3a**). It is worth noting that because the inert solvent of OFE cannot highly coordinate with Li^+ ion to obtain solvation-Li^+ complex, the overpotential in such a LHCE of DME5 is slightly larger than that of dilute electrolyte at the beginning. However, the enlarged profiles of Li metal plating/stripping exhibit a favorable Li metal exchange with a constant overpotential of ~ 0.2 V no matter at the begining, the middle or the end of cycling (**Figure S3b**). In comparison, as displayed in **Figure S3c-d**, the voltage polarization gradually increases during continuous cycling under the same test conditions. Especially for the DME15 eletrolyte, the Li|Li cells shows the electrode overpotential is about 0.4 V at 600h, twice as large as the DME5, indicating a increased interfacial reaction resistances. The comparison results demonstrate that the impedance in DME15 and DME50 electrolytes with a large amount of free DME solvent continuously increased probably due to the remarkable side reactions between electrolyte and Li dendrite, but it was obviously restrained in DME5

electrolyte by suppression of Li dendrite. Besides, because of the introduction of the inert OFE coslovent, the overpotential for Li plating/stripping cycling in the OFE cosolvent electrolyte system is higher than the some published works with dilute electrolyte systems,[16] but the introduction of inert OFE solvent into the HCE system can obtain a new class of LHCE system without breaking the unique Li^+ solvation structure complexes of HCE, leading to minimum free active solvent in the LHCE. Therefore, the excellent cycling stability of Li metal plating/stripping along with stable overpotential verifies that the rational introduction of OFE dilution in the electrolyte can effectively supress the Li dendrite, enabling the stable Li deposition/stripping cycles.

2.4. Mechanisms for Li dendrite suppression in Li Deposition/Stripping cycles

In order to reveal the stable Li deposition/stripping mechanism in such a LHCE of DME5, X-ray photoelectron spectroscopy analysis (XPS) with Ar^+ etching technique was performed to analyze the SEI layer on the Li anode surfaces formed in the DME5 and DME50 electrolytes, respectively. The atomic concentration for different elements along with increasing etching time are demonstrated in **Figure 4a-b** and **Table S2**. It can be clearly found that the chemical composition of SEI layer in the DME5 maintains a higher atomic concentration of F and Li elements when compared with that in DME50 electrolyte. This atom concentration tendency in the SEI layer formed in DME5 electrolyte is similar to that of SEI layer formed in typical HCEs.[15b] Furthermore, the high-resolution Li 1s XPS spectra for DEM5 and DME50 in **Figure 4c** show an obvious negative shift of the peak position with the etching time increasing from 0 s to 1200 s, which should be attributed to the sequential appearance of low-binding-energy Li-O bonds at around 55.5 ± 0.5 eV and lithium metal (Li^0) at around 53.0 ± 0.5 eV along with the increased etching depth. More importantly, it can be

clearly observed that the content of Li-F bonds at around 58.0 ± 0.5 eV significantly increased for the SEI layer formed in the DME5 electrolyte, especially at the etching time of 100 s and 300 s, while Li-O bond is the dominated type for element Li in the SEI layer formed in the DME50 electrolyte.

The signal of Li-F bond can also be observed in the F1s XPS spectra for the both DME5 and DME50 electrolytes, as shown in **Figure 4d**. A main peak at about 685.7 eV can be found for both DME5 and DME50 electrolytes, suggesting that the F element in the SEI layer mainly exists in the form of F-Li bond. The peak at around 688.4 eV was assigned to F-C bonds, which should be mainly attributed to the adsorption of the fluorine-rich OFE solvent. Moreover, the intensity of Li-F peak is significantly enhanced for the SEI layer formed in the DME 5 electrolyte when compared with that in DME 50 electrolyte. It can be deduced that a much higher content of inorganic LiF phase in the SEI layer was formed in DME5 electrolyte than that in DME50 electrolyte.

These results indicated that such a LHCE of DME5 can well maintain the similar solvation structure and unique function to typical HCE systems and then promote more F-containing components (such as FSI^- anion and OFE solvent) participating in the formation of SEI layer, resluting to a dense and stable LiF-rich SEI layer which can significantly suppress the Li dendrite growth.[17] In addition, such a LHCE electrolyte of DME5 electrolyte also shows excellent properties of lower cost, lower viscosity, and better wettability than that of typical HCE systems, making it more advantage for practical application in Li-S batteries.

2.5. Electrochemical Behavior of S@C (65.02 wt.% for S) Cathodes

In order to further investigate the electrochemical equilibria of S@C cathodes during discharge/charge process in various electrolytes, galvanostatic intermittent titration techniques (GITT) were performed in the voltage window 1-3 V after 15 activation cycles, by applying a

short pulses of constant current of 100 mA/g for 20min then leaving in open-circuit of 2h for full relaxations to reach equilibrium potential. **Figure 5a-b** represented the GITT profiles of Li-S cells in the DME5 and DME50 electrolytes, respectively. It can be found that the discharge curve of open circuit voltage (OCV) in DME5 electrolyte only has one plateau, and the voltage polerization of S cathode is large but remains almost constant, indicating a deep and direct reduction reaction from solid S_8 to solid-state Li_2S.[18] In contrast, two plateaus regions at about 2.30 V and 2.15 V, similar to the S cathodes in a dilute electrolyte, appear in DME50 electrolyte, corresponding to the conversion reaction of solid S_8 to soluble high-order Li_2S_m and then to insoluble low-order Li_2S_2/Li_2S, respectively.[19] Moreover, the voltage polarization of S cathode in DME50 electrolyte increase with state of discharge increased in reaction resistance from soluble liquid low-order lithium polysulfide to insoluble solid Li_2S_2/Li_2S.[20] The voltage polarization of S cathode at the end of the lower voltage region is similar to that in DME5 elecyrolyte, due to the slow kinetics of solid-solid two phase reduction reaction between Li_2S_2 adn Li_2S. More importantly, during charge in the DME50 electrolyte, a large voltage polarization is observed at the initial de-lithiation from solid Li_2S to solid Li_2S_2 process, then decreasing gradually due to solid-liquid and keeping at a small but constant overpotential in liquid-liquid shuttle reaction, which is the notorious shuttle phenomenon in Li-S batteries. But for the GITT profile in DME5 electrolyte, the state of electrochemical equilibration is reversible without any shuttle. Furthermore, five sequential and stable GITT profile after 15 discharge/charge activation cycles in **Figure S4** obviously demonstrated the thermodynamically suppression of shuttle phenomenon by the addition of appropriate OFE inert solvent in the DME5.

Furthermore, the self-discharge phenomenon, mainly caused by the shuttle reaction of soluble lithium polysulfides migratation from cathode side, is one of the most severe issues

that hinder further practical application of Li-S batteries, leading to obvious decrease of OCV and loss of discharge capacity.[21] Thus, the inhibition of the shuttle reaction in turn can reduce the self-discharge rate of Li-S battery, owing to its effective suppression of polysulfides dissolution and migration. Here the self-dischage property of Li-S batteries in different electrolytes was evaluated after 20 activation discharging/charging cycles at the current of 50 mA/g by fully charging Li-S cells, leaving in open-circuit for a long-term rest period of 60 days, and then discharging at the same current. **Figure 5c-e** are the comparison of the self-discharge rate of Li-S batteries based on the capacity loss in the OFE-based electrolytes. The battery in the DME5 electrolyte maintains the lowest capacity loss of 16.9% after rest for 60 days (**Figure 5c**), but a high capacity loss of 29.5% for DME15 (**Figure 5d**) and a very severe capacity loss of 50.6% for DME50 (**Figure 5e**). The excellent capacity recovery in DME5 electrolyte is consistent with the significant suppression of shuttle reaction in DME5 via the maximun addition of OFE along with minimum low solubility of polysulfides, which can effectively improve the CE of sulfur cathode and give a promise of practical application of long-term high-performance Li–S batteries. These results can be attributed to the less and less polysulfide dissolution along with the increasing OFE content into the LiFSI/DME electrolytes, which are well consistent with the UV-Vis results.

Cyclic voltammetry (CV) scans were first used to identify the redox reactions process of S@C composites (**Figure S5**) in various electrolytes, as shown in **Figure 6a**. During the cathodic scan, the CV curves of the S@C in DME5 possess one main reduction peaks, which can be ascribed to the direct reduction of solid insoluble elemental sulfur to insoluble low-order polysulfide because of no free DME solvent to dissolve the high-oder polysulfide in the LHCE of DME5. This unique redox behaviour can also be confirmed by the charge-discharge curves in DME5 in **Figure 6b**, which possess only one plateau at its 2nd cycling. In the

subsequent anodic scan, there is also only one oxidation peak at about 2.70 V, which can be atrribiuted to the oxidation conversion of Li_2S_2/Li_2S into elemental sulphur in DME5 electrolyte. These phenomena in the DME5 electrolyte agrees with the obvious reports for the highly concentrated electrolyte.[19, 22]

In contrast, for the CV curves of the S@C in DME15 electrolyte, two typical reduction peaks clearly appear, which is related to the reduction of solid sulfur to liquid high-order polysulfides and further reduction of higher-order polysulfides to solid insoluble Li_2S_2/Li_2S, respectively. Accordingly, the 2nd discharge curve in DME15 reflects two plateaus attributed to the two step reduction process. Furthermore, owing to the high activity of adundant DME in DME50 electrolyte, three main reduction peaks at about 2.29 V, 2.02 V and 1.78 V were observed in the CV curves for DME50, corresponding to the reduction of solid S to liquid high-order polysulfides, higher-order polysulfides to lower-order polysulfides, and deep reduction of polysulfide to Li_2S, respectively.[23] The coresponding discharge curve of DME50 in **Figure 6b** (bottom) also shows two obvious plateaus are apeared at around 2.31 V and 2.09 V with a slop tail for formation of Li_2S, in accordance with the previously reported dilute electrolytes for Li-S batteries.[18b] Importantly, the upper voltage plateau in DME50 is much more longer (higher capacity) than that in DME15, indicating the higher dissolution of higher-order polysulfides in DME50 with sufficient free DME solvent.

These different electrochemical behaviors in the OFE-based electrolytes are related to competetive solvation for Li^+ by solvents and FSI^- anions. Due to the different salt concentration and the structure of solvent and anions of electrolyte, the competition leads to various Li^+-solvation species from the SSIPs, CIPs, to AGGs with the increasing of concentration. In the LHCE, the solvation species is priority to generate the AGGs, hardly with any free solvent. Therefore, a quasi-solid-state reaction mechanism in LHCE will

dominate the Li-S chemistry as compared with another reaction of solid-liquid-solid in dilute electrolyte.[24] As a result, the dissolution of high-order polysulfides in DME5 can be completely inhibited without upper CV peaks and corresponding discharge plateaus; while for the solid-liquid-solid mechanism in DME15 and DME50 electrolytes, there are evident upper-voltage peaks and plateaus corresponding to the polysulfides dissolution process. Moreover, when comparing the dischaging/charging beheviors in various OFE-based electrolyte at 1st, 2nd and 150th cycles in **Figure 6b-c** and **Figure S6**, it can be obviously found that in the DME5 electrolyte, the discharge capacity is slightly higher than the charge capacity at 1st and 2nd cycles which should be attributed to the irreversible formation of SEI during the initial few discharge/charge cycles. After that, the capacity difference decreased, and ~100% of CE is achieved after 10 cycles (**Figure S7**). But for the electrolyte of DME15 and DME50, the discharge capacity is lower than the charge capacity no matter from the 1st, 2nd, to 150th with the CE of $>$ 100% (CE= charge capacity/discharge capacity). The obvious comparison indicates the existence of obvious shuttle effect in these dilute electrolytes of DME15 and DME50 but complete disappearance of shuttle effect in the LHCE of DME5. As a result, based on the CV redox peak signal and upper-voltage plateau in discharge curve, the polysulfide shuttle can be stepwise controlled only by gradually adjusting the OFE cosolvent content in these OFE-based electrolytes.

Figure 6d shows the cycling performance of S@C cathodes at a current density of 100 mA/g in various electrolytes. The DME5 electrolyte depicts the best cycling stability, maintaining a reversible discharge capacity of 775 mAh/g for 150th cycling with the initial CE of 83% and the average CE of 99.2%; while the DME15 possess 633 mAh/g, DME50 with 314 mAh/g, and DOL+DME with 458 mAh/g under the same conditions. For these dilute electrolytes of DME15, DME50, and DOL+DME, their corresponding CE are all greater than

100% during all cycles, as indicated in the **Figure S7**. More specifically, in the dilute electrolyte of DME50, there is a CE of 116% at the initial cycle and the average CE of > 100%, which is attributed to the shuttle effect in the dilute electrolytes that transfer the high-order polysulfide through the separator to Li anode surface with irreversible consumption of the active material and electrolyte, leading to the rapid capacity fading and shuttle-reaction CE of more than 100%. Besides, as shown in **Figure 6e**, the Li-S battery with the DME5 electrolyte also shows excellent rate performance, with the discharge capacities of 1012, 823, 666, 402 and 223 mAh/g at current densities of 0.05, 0.1, 0.5, 2.0 and 4.0 A/g, respectively. When the current density switches back from 4.0 A/g to 0.1 A/g, the discharge capacity maintains at 774 mAh/g, almost returning to its original capacity even after cycling at high current density, implying the superior reversibility and excellent tolerance of high-rate capability in the DME5 electrolyte.

Importantly, owing to significant suppression of dissolution of polysulfide in DME5 electrolyte with the excellent high CE of 99.2% for S@/C cathode and 99.3% CE for Li anode, the amount of electrolyte using for the Li-S batteries was reduced to 4.56 g/Ah, which is much lower than that of most previous reported value for Li-S batteries, accompanied with much better commercial application.

Based on the above results and analysis, it can be concluded that the excellent electrochemical performance of the Li-S batteries in the LHCE of DME5 is ascribed to the following two reasons: (i) the formation of robust SEI layer with rich LiF component on the surface of Li metal anode from reduction of OFE and FSI^- which can effectively suppress Li dendrite growth and promote Li plating/stripping reversibility; (ii) the shuttle reaction in Li-S chemistry is completely inhibited via introduction of the inert OFE cosolvent with low donor number for Li salt and minimum ability for dissolution polysulfides. The two advantages in

the LHCE of DME5 promise a significant improvement of electrochemical performance for Li-S batteries.

3. Conclusion

In summary, a localized high-concentration OFE-based electrolyte was firstly developed by using the inert fluoroalkyl ether OFE as the cosolvent diluent in 1M LiFSI/OFE+DME. We have successfully suppressed the Li dendrite growth and polysulfide shuttle reaction in Li-S batteries. As the most effective electrolyte for Li-S cells, the DME5 electrolytes shows its outstanding performance, which can simultaneously enable both the formation of dendrite-free Li cycling with a high CE up to 99.3% and completely suppression of shuttling effect of lithium polysulfide with stable cycling for the S cathode (99.2% of CE). When compared with the typical HCEs, this diffcult burning LHCE of DME5 not only possess the superior solvation structure and unique function for the formation of LiF-rich SEI layer, but also maintains a lower cost, lower viscosity, and better wettability, making it more advantage for further application in Li-S batteries. The fundamental concept of LHCE can also be widely extended to many other battery systems, such as the Li metal batteries, Na (K) metal batteries, and sulfur-based metal ion batteries. Therefore, it opens a new horizon for the further development of advanced electrolyte systems for next-generation energy storage technologies.

Supporting Information

Supplementary data associated with this article can be found in the online version.

Acknowledgements

The authors thank the support from the Nanostructures for Electrical Energy Storage (NEES), an Energy Frontier Research Center funded by the U.S. Department of Energy, Office of Science, Basic Energy Sciences under Award number DESC0001160. The authors gratefully acknowledge the support of the Maryland NanoCenter and its AIM Lab.

Conflict of Interest

The authors declare no competing financial interest.

Received: ((will be filled in by the editorial staff))
Revised: ((will be filled in by the editorial staff))
Published online: ((will be filled in by the editorial staff))

References

[1] A. Manthiram, Y. Fu, S.-H. Chung, C. Zu, Y.-S. Su, *Chem. Rev.* **2014**, 114, 11751.

[2] a) J. Qian, W. A. Henderson, W. Xu, P. Bhattacharya, M. Engelhard, O. Borodin, J.-G. Zhang, *Nat. Commun.* **2015**, 6, 6362; b) N. S. Choi, Z. Chen, S. A. Freunberger, X. Ji, Y. K. Sun, K. Amine, G. Yushin, L. F. Nazar, J. Cho, P. G. Bruce, *Angew. Chem. Inte. Edi.* **2012**, 51, 9994; c) L. Suo, Y.-S. Hu, H. Li, M. Armand, L. Chen, *Nat. commun.* **2013**, 4, 1481.

[3] a) L. Ji, M. Rao, H. Zheng, L. Zhang, Y. Li, W. Duan, J. Guo, E. J. Cairns, Y. Zhang, *J. Am. Chem. Soc.* **2011**, 133, 18522; b) T. Lin, Y. Tang, Y. Wang, H. Bi, Z. Liu, F. Huang, X. Xie, M. Jiang, *Energ. & Environ. Sci.* **2013**, 6, 1283.

[4] a) X. Ji, K. T. Lee, L. F. Nazar, *Nat. Mater.* **2009**, 8, 500; b) S. Moon, Y. H. Jung, W. K. Jung, D. S. Jung, J. W. Choi, D. K. Kim, *Adv. Mater.* **2013**, 25, 6547.

[5] L. Xiao, Y. Cao, J. Xiao, B. Schwenzer, M. H. Engelhard, L. V. Saraf, Z. Nie, G. J. Exarhos, J. Liu, *Adv. Mater.* **2012**, 24, 1176.

[6] a) K. Yan, Z. Lu, H.-W. Lee, F. Xiong, P.-C. Hsu, Y. Li, J. Zhao, S. Chu, Y. Cui, *Nat. Energ.* **2016**, 1, 16010; b) G. Zheng, S. W. Lee, Z. Liang, H.-W. Lee, K. Yan, H. Yao, H. Wang, W. Li, S. Chu, Y. Cui, *Nat. nanotechnol.* **2014**, 9, 618; c) D. Lin, Y. Liu, Z.

Liang, H.-W. Lee, J. Sun, H. Wang, K. Yan, J. Xie, Y. Cui, *Nat. nanotechnol.* **2016**, 11, 626.

[7] N. W. Li, Y. X. Yin, C. P. Yang, Y. G. Guo, *Adv. Mater.* **2016**, 28, 1853.

[8] a) Y. Liping, M. Jun, Z. Jianjun, Z. Jingwen, D. Shanmu, L. Zhihong, C. Guanglei, C. Liquan, *Energy Storage Mater.* **2016**, 5, 139; b) G. Xu, C. Pang, B. Chen, J. Ma, X. Wang, J. Chai, Q. Wang, W. An, X. Zhou, G. Cui, L. Chen, *Adv. Energy Mater.* **2018**, 8, 1701398.

[9] S. Zhang, K. Ueno, K. Dokko, M. Watanabe, *Adv. Energ. Mater.* **2015**, 5, 1500117.

[10] a) J. Zheng, S. Chen, W. Zhao, J. Song, M. H. Engelhard, J.-G. Zhang, *ACS Energy Lett.* **2018**, 3, 315; b) S. Chen, J. Zheng, D. Mei, K. S. Han, M. H. Engelhard, W. Zhao, W. Xu, J. Liu, J. G. Zhang, *Adv. Mater.* **2018**, 30, 1706102.

[11] a) K. Dokko, N. Tachikawa, K. Yamauchi, M. Tsuchiya, A. Yamazaki, E. Takashima, J.-W. Park, K. Ueno, S. Seki, N. Serizawa, *J. Electrochem. Soc.* **2013**, 160, A1304; b) T. Doi, Y. Shimizu, M. Hashinokuchi, M. Inaba, *J. Electrochem. Soc.* **2017**, 164, A6412.

[12] R. Cao, W. Xu, D. Lv, J. Xiao, J. G. Zhang, *Adv. Energ. Mater.* **2015**, 5, 1402273.

[13] H. Moon, T. Mandai, R. Tatara, K. Ueno, A. Yamazaki, K. Yoshida, S. Seki, K. Dokko, M. Watanabe, *J. Phys. Chem. C* **2015**, 119, 3957.

[14] a) Y. Yamada, A. Yamada, *J. Electrochem. Soc.* **2015**, 162, A2406; b) O. Borodin, L. Suo, M. Gobet, X. Ren, F. Wang, A. Faraone, J. Peng, M. Olguin, M. Schroeder, M. S. Ding, *ACS nano* **2017**, 11, 10462.

[15] a) M. Shin, H.-L. Wu, B. Narayanan, K. A. See, R. S. Assary, L. Zhu, R. T. Haasch, S. Zhang, Z. Zhang, L. A. Curtiss, *ACS appl. Mater. Inter.* **2017**, 9, 39357; b) J. Zheng,

X. Fan, G. Ji, H. Wang, S. Hou, K. C. DeMella, S. R. Raghavan, J. Wang, K. Xu, C. Wang, *Nano Energy* **2018**.

[16] a) J. Qian, W. A. Henderson, W. Xu, P. Bhattacharya, M. Engelhard, O. Borodin, J.-G. Zhang, *Nat. Commun.* **2015**, 6; b) G. Bieker, M. Winter, P. Bieker, *Phys. Chem. Chem. Phys.* **2015**, 17, 8670; c) M. S. Park, S. B. Ma, D. J. Lee, D. Im, S.-G. Doo, O. Yamamoto, *Sci. Rep.* **2014**, 4.

[17] J. Zheng, J. A. Lochala, A. Kwok, Z. D. Deng, J. Xiao, *Adv. Sci.* **2017**, 4, 1700032.

[18] a) S. S. Zhang, *Front. Energy Res.* **2013**, 1, 10; b) S. S. Zhang, *J. Power Sources* **2013**, 231, 153.

[19] M. Cuisinier, P.-E. Cabelguen, B. Adams, A. Garsuch, M. Balasubramanian, L. Nazar, *Energ. Environ. Sci.* **2014**, 7, 2697.

[20] J.-W. Park, K. Yamauchi, E. Takashima, N. Tachikawa, K. Ueno, K. Dokko, M. Watanabe, *J. Phys. Chem. C* **2013**, 117, 4431.

[21] F. Jeschull, D. Brandell, K. Edström, M. J. Lacey, *Chem. Commun.* **2015**, 51, 17100.

[22] M. Cuisinier, P.-E. Cabelguen, S. Evers, G. He, M. Kolbeck, A. Garsuch, T. Bolin, M. Balasubramanian, L. F. Nazar, *J. Phys. Chem. Lett.* **2013**, 4, 3227.

[23] C. Barchasz, F. Molton, C. Duboc, J.-C. Leprêtre, S. b. Patoux, F. Alloin, *Anal. Chem.* **2012**, 84, 3973.

[24] D.-W. Wang, Q. Zeng, G. Zhou, L. Yin, F. Li, H.-M. Cheng, I. R. Gentle, G. Q. M. Lu, *J. Mater. Chem. A* **2013**, 1, 9382.

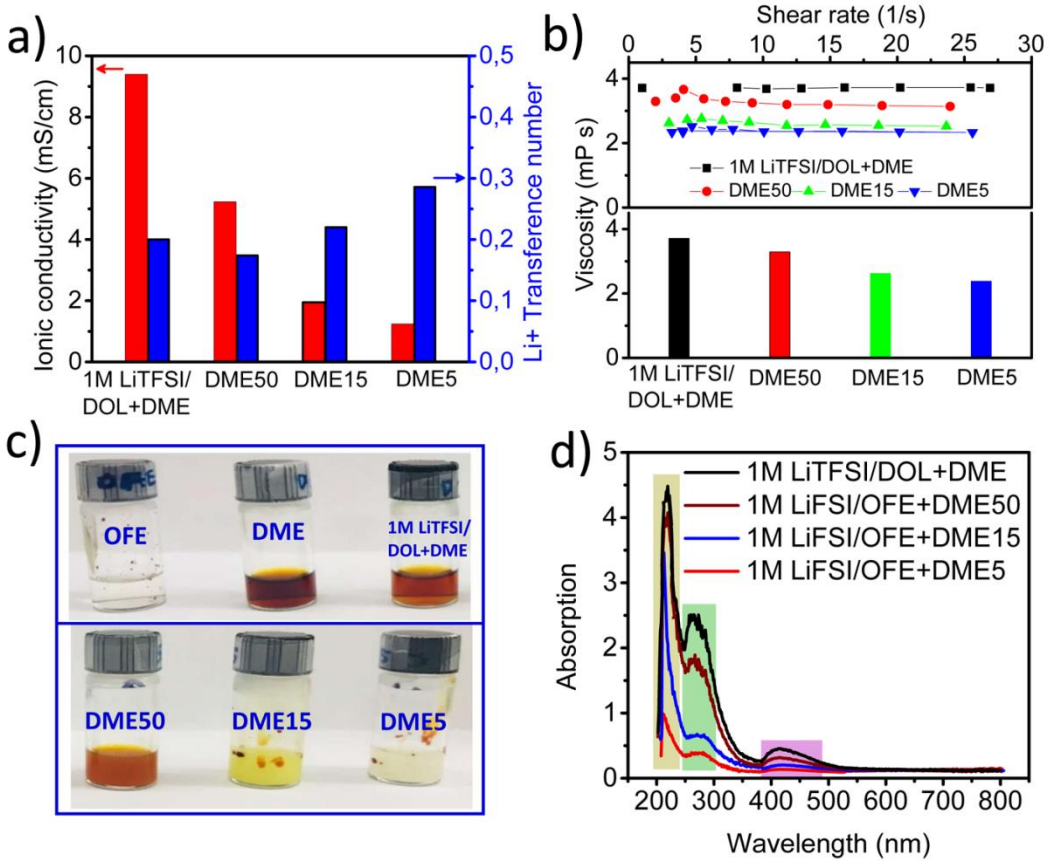

Figure 1 Physicochemical parameters for various electrolytes: a) Li^+ transference number and ionic conductivity; b) electrolyte viscosities as functions of shear-rate (top) and the corresponding average viscosities (bottom). c, d) Property of lithium polysulfide dissolution: c) digital photos for saturate Li_2S_8 in different solutions after 2 weeks standing, and d) the corresponding UV-Vis absorption spectra.

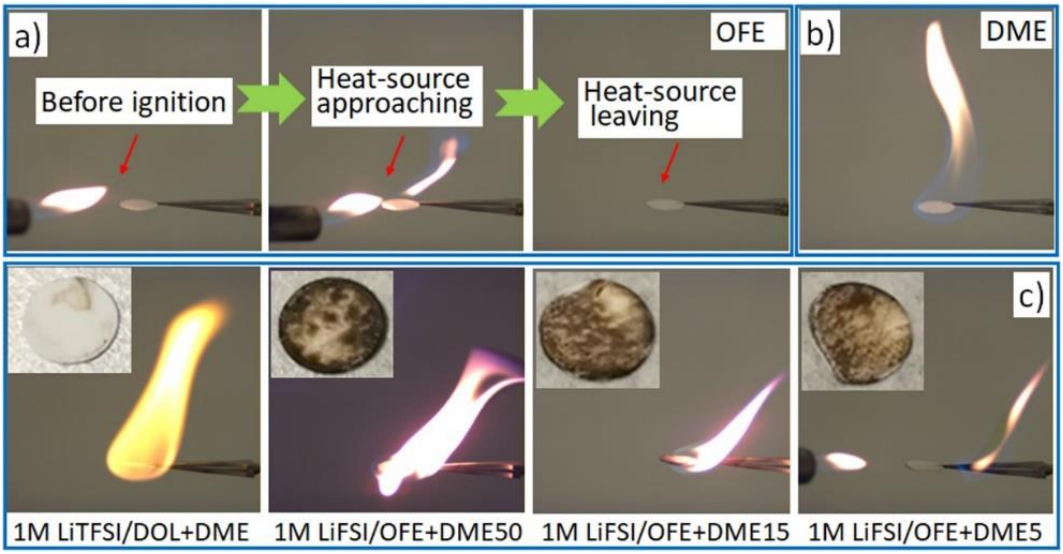

Figure 2 The ignition and combustion experiment: the ignition process for the solvents of a) OFE and b) DME; c) the combustion flammability for various electrolytes on glass fiber films (inset: the images of glass-fiber films after combustion).

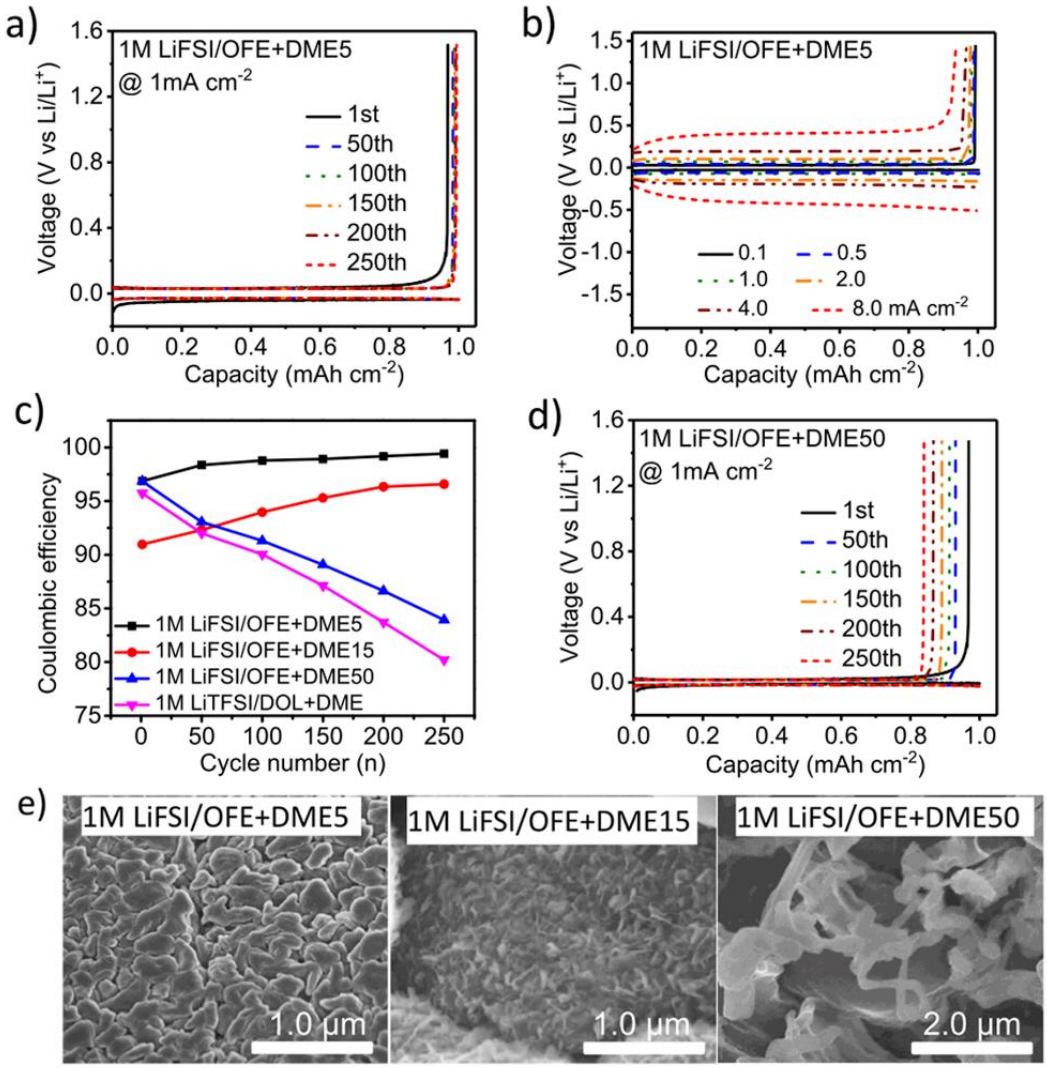

Figure 3 Voltage profiles for Li plating/stripping on Cu working electrode (Li|Cu cell) in 1M LiFSI/OFE+DME5 electrolyte a) at the current density of 1.0 mA cm^{-2} and b) at different current densities with the deposition capacity of 1.0 mAh cm^{-2}; c) comparison of Li deposition CE at 1.0 mA cm^{-2} during 250 cycles in different electrolytes; d) voltage profile of Li metal deposition/stripping at 1.0 mA cm^{-2} with the same deposition capacity of 1.0 mAh cm^{-2} in dilute 1M LiFSI/OFE+DME50 electrolyte; e) SEM images of the Li metal surface in the OFE-based electrolytes after 100 cycles at the current of 1.0 mA cm^{-2} in Li|Cu cells.

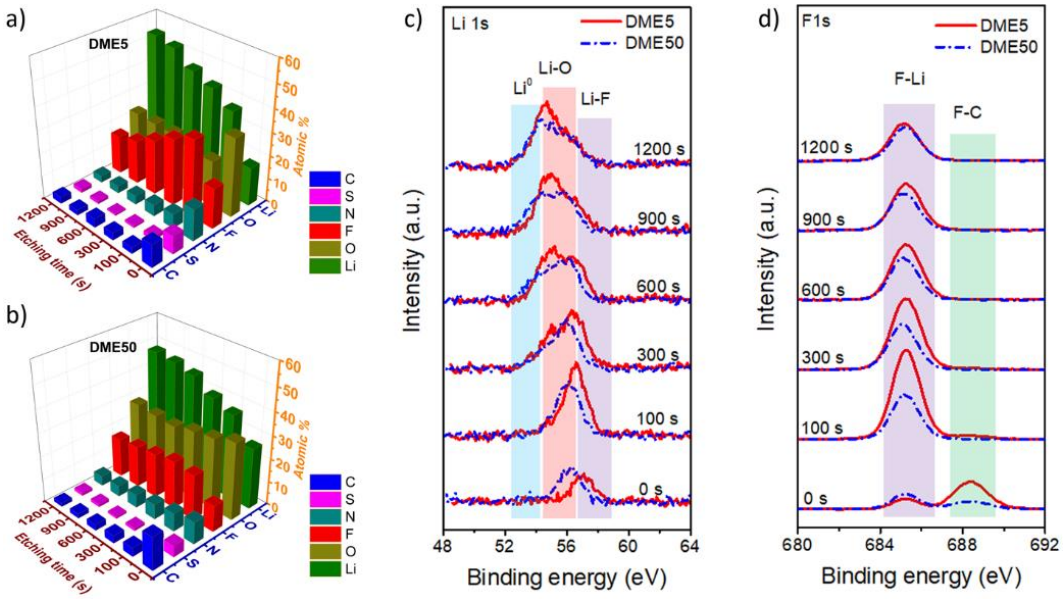

Figure 4 X-ray photoelectron spectroscopy (XPS) analysis for Li metal surface in Li|Cu cells at the current of 100 mA/g after 50 cycles: a, b) atomic concentrations for different elements before and after different etching times in a) 1M LiFSI/OFE+DME5 and b) 1M LiFSI/OFE+DME50 electrolytes; c, d) high-resolution spectra of c) Li 1s XPS and d) F1s XPS for the lithium metal surface in 1M LiFSI/OFE+DME5 and 1M LiFSI/OFE+DME50 electrolytes.

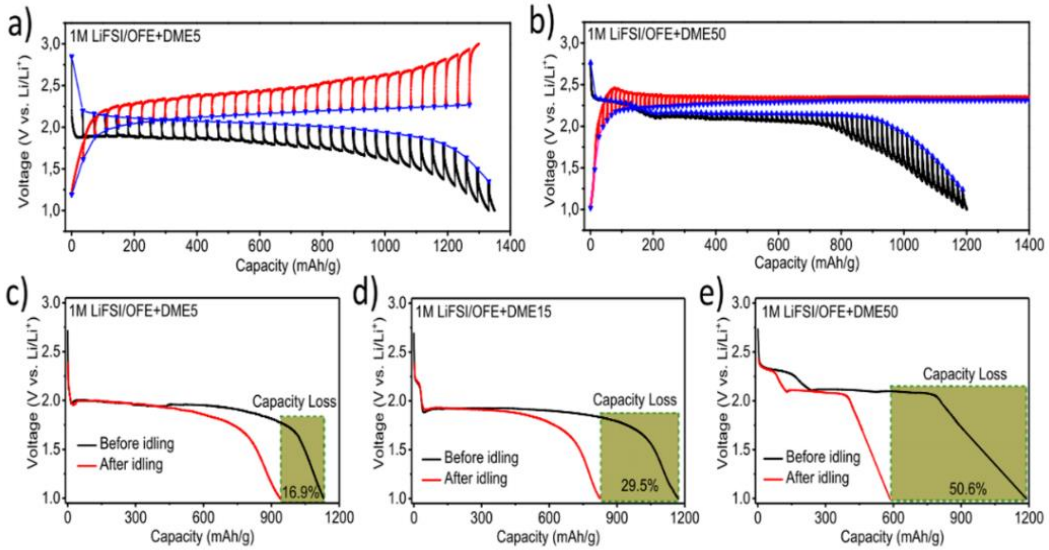

Figure 5 GITT curves in a) 1M LiFSI/OFE+DME5 and b) 1M LiFSI/OFE+DME50 electrolyte; c-d) long-term self-discharge characteristics: discharge curves for Li-S cells before (black curve) and after (red curve) iding for 60 days in c) 1M LiFSI/OFE+DME5, d) 1M LiFSI/OFE+DME15 and e) 1M LiFSI/OFE+DME50 electrolytes.

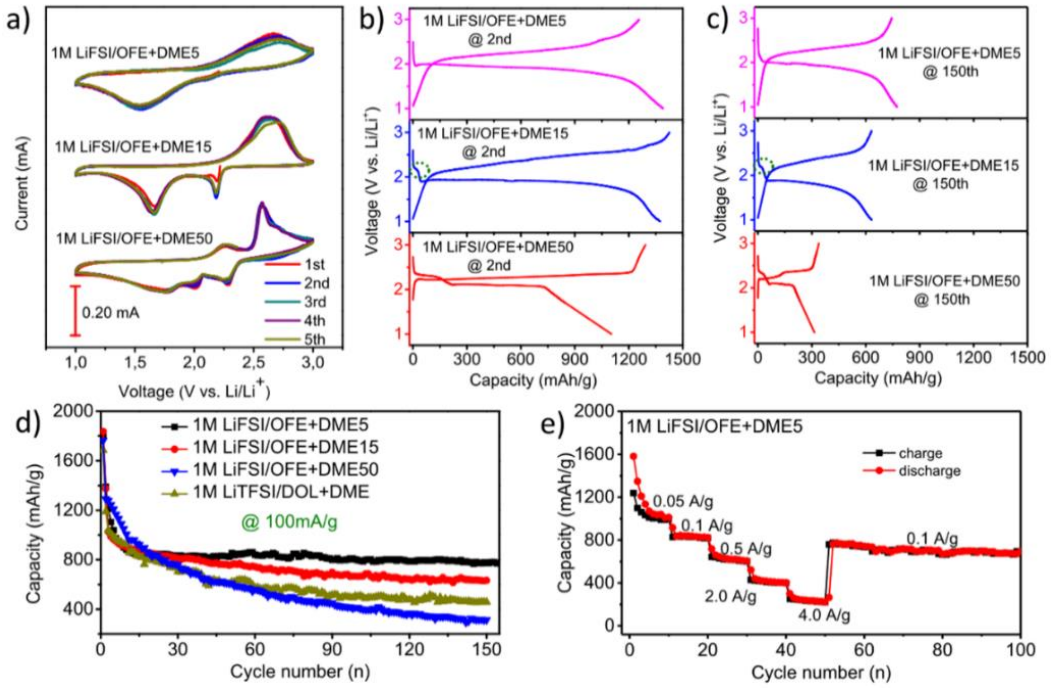

Figure 6 Electrochemical performance: a) cyclic voltammogram in different electrolytes at 0.05 mV/s; charge-discharge curves with current density of 100 mA/g at b) 2nd and c) 150th cycling; d) comparison of specific discharge capacity at 100 mA/g in different electrolytes; e) the rate performance of Li-S batteries with 1M LiFSI/OFE+DME5 electrolyte.

The table of contents:

A new class of non-flammable localized high-concentration electrolyte (LHCE) with similar superior solvation structures and unique functions but lower cost, smaller viscosity, and better wettability than traditional HCE systems was rationally designed to control the Li-S chemistry, simultaneously suppressing the shuttle effect of lithium polysulfide and growth of lithium dendrites with minimized usage of electrolyte of 4.56 g/Ah in Li-S batteries.

Keyword: inert fluorinated diluents, localized high-concentration electrolyte, polysulfide shuttle, lithium dendrite, Li-S batteries

J. Zheng, G. Ji, X. Fan, J. Chen, Q Li, H. Wang, Y. Yang, K. C. DeMella, S. R. Raghavan, C. Wang*

Title: High-Fluorinated Electrolytes for Li-S Batteries

ToC figure

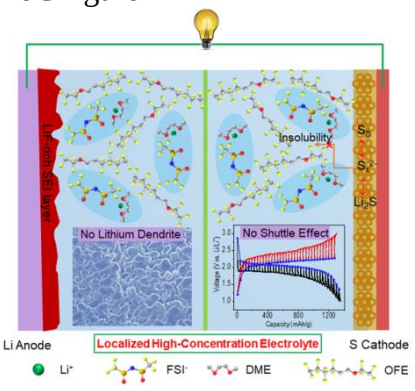

[1] A. Manthiram, Y. Fu, S.-H. Chung, C. Zu, Y.-S. Su, *Chemical reviews* **2014**, 114, 11751.

[2] a) J. Qian, W. A. Henderson, W. Xu, P. Bhattacharya, M. Engelhard, O. Borodin, J.-G. Zhang, *Nature communications* **2015**, 6, 6362; b) N. S. Choi, Z. Chen, S. A. Freunberger, X. Ji, Y. K. Sun, K. Amine, G. Yushin, L. F. Nazar, J. Cho, P. G. Bruce, *Angewandte Chemie International Edition* **2012**, 51, 9994; c) L. Suo, Y.-S. Hu, H. Li, M. Armand, L. Chen, *Nature communications* **2013**, 4, 1481.

[3] a) L. Ji, M. Rao, H. Zheng, L. Zhang, Y. Li, W. Duan, J. Guo, E. J. Cairns, Y. Zhang, *Journal of the American Chemical Society* **2011**, 133, 18522; b) T. Lin, Y. Tang, Y. Wang, H. Bi, Z. Liu, F. Huang, X. Xie, M. Jiang, *Energy & Environmental Science* **2013**, 6, 1283.

[4] a) X. Ji, K. T. Lee, L. F. Nazar, *Nature materials* **2009**, 8, 500; b) S. Moon, Y. H. Jung, W. K. Jung, D. S. Jung, J. W. Choi, D. K. Kim, *Advanced Materials* **2013**, 25, 6547.

[5] L. Xiao, Y. Cao, J. Xiao, B. Schwenzer, M. H. Engelhard, L. V. Saraf, Z. Nie, G. J. Exarhos, J. Liu, *Advanced materials* **2012**, 24, 1176.

[6] a) K. Yan, Z. Lu, H.-W. Lee, F. Xiong, P.-C. Hsu, Y. Li, J. Zhao, S. Chu, Y. Cui, *Nature Energy* **2016**, 1, 16010; b) G. Zheng, S. W. Lee, Z. Liang, H.-W. Lee, K. Yan, H. Yao, H. Wang, W. Li, S. Chu, Y. Cui, *Nature nanotechnology* **2014**, 9, 618; c) D. Lin, Y. Liu, Z. Liang, H.-W. Lee, J. Sun, H. Wang, K. Yan, J. Xie, Y. Cui, *Nature nanotechnology* **2016**, 11, 626.

[7] N. W. Li, Y. X. Yin, C. P. Yang, Y. G. Guo, *Advanced Materials* **2016**, 28, 1853.

[8] a) Y. Liping, M. Jun, Z. Jianjun, Z. Jingwen, D. Shanmu, L. Zhihong, C. Guanglei, C. Liquan, *Energy Storage Materials* **2016**, 5, 139; b) G. Xu, C. Pang, B. Chen, J. Ma, X. Wang, J. Chai, Q. Wang, W. An, X. Zhou, G. Cui, L. Chen, *Advanced Energy Materials* **2018**, 8, 1701398.

[9] S. Zhang, K. Ueno, K. Dokko, M. Watanabe, *Advanced Energy Materials* **2015**, 5, 1500117.

[10] a) J. Zheng, S. Chen, W. Zhao, J. Song, M. H. Engelhard, J.-G. Zhang, *ACS Energy Letters* **2018**, 3, 315; b) S. Chen, J. Zheng, D. Mei, K. S. Han, M. H. Engelhard, W. Zhao, W. Xu, J. Liu, J. G. Zhang, *Advanced Materials* **2018**, 30, 1706102.

[11] a) K. Dokko, N. Tachikawa, K. Yamauchi, M. Tsuchiya, A. Yamazaki, E. Takashima, J.-W. Park, K. Ueno, S. Seki, N. Serizawa, *Journal of The Electrochemical Society* **2013**, 160, A1304; b) T. Doi, Y. Shimizu, M. Hashinokuchi, M. Inaba, *Journal of The Electrochemical Society* **2017**, 164, A6412.

[12] R. Cao, W. Xu, D. Lv, J. Xiao, J. G. Zhang, *Advanced Energy Materials* **2015**, 5, 1402273.

[13] H. Moon, T. Mandai, R. Tatara, K. Ueno, A. Yamazaki, K. Yoshida, S. Seki, K. Dokko, M. Watanabe, *The Journal of Physical Chemistry C* **2015**, 119, 3957.

[14] a) Y. Yamada, A. Yamada, *Journal of The Electrochemical Society* **2015**, 162, A2406; b) O. Borodin, L. Suo, M. Gobet, X. Ren, F. Wang, A. Faraone, J. Peng, M. Olguin, M. Schroeder, M. S. Ding, *ACS nano* **2017**, 11, 10462.

[15] a) M. Shin, H.-L. Wu, B. Narayanan, K. A. See, R. S. Assary, L. Zhu, R. T. Haasch, S. Zhang, Z. Zhang, L. A. Curtiss, *ACS applied materials & interfaces* **2017**, 9, 39357; b) J. Zheng, X. Fan, G. Ji, H. Wang, S. Hou, K. C. DeMella, S. R. Raghavan, J. Wang, K. Xu, C. Wang, *Nano Energy* **2018**.

[16] a) J. Qian, W. A. Henderson, W. Xu, P. Bhattacharya, M. Engelhard, O. Borodin, J.-G. Zhang, *Nature Communications* **2015**, 6; b) G. Bieker, M. Winter, P. Bieker, *Physical Chemistry Chemical Physics* **2015**, 17, 8670; c) M. S. Park, S. B. Ma, D. J. Lee, D. Im, S.-G. Doo, O. Yamamoto, *Scientific Reports* **2014**, 4.

[17] J. Zheng, J. A. Lochala, A. Kwok, Z. D. Deng, J. Xiao, *Advanced Science* **2017**, 4, 1700032.

[18] a) S. S. Zhang, *Frontiers in Energy Research* **2013**, 1, 10; b) S. S. Zhang, *Journal of Power Sources* **2013**, 231, 153.

[19] M. Cuisinier, P.-E. Cabelguen, B. Adams, A. Garsuch, M. Balasubramanian, L. Nazar, *Energy & Environmental Science* **2014**, 7, 2697.

[20] J.-W. Park, K. Yamauchi, E. Takashima, N. Tachikawa, K. Ueno, K. Dokko, M. Watanabe, *The Journal of Physical Chemistry C* **2013**, 117, 4431.

[21] F. Jeschull, D. Brandell, K. Edström, M. J. Lacey, *Chemical Communications* **2015**, 51, 17100.

[22] M. Cuisinier, P.-E. Cabelguen, S. Evers, G. He, M. Kolbeck, A. Garsuch, T. Bolin, M. Balasubramanian, L. F. Nazar, *The Journal of Physical Chemistry Letters* **2013**, 4, 3227.

[23] C. Barchasz, F. Molton, C. Duboc, J.-C. Leprêtre, S. b. Patoux, F. Alloin, *Analytical chemistry* **2012**, 84, 3973.

[24] D.-W. Wang, Q. Zeng, G. Zhou, L. Yin, F. Li, H.-M. Cheng, I. R. Gentle, G. Q. M. Lu, *Journal of Materials Chemistry A* **2013**, 1, 9382.